

The role of feedback in accretion on low-luminosity AGN: Sgr A* case study

Jorge Cuadra,^{1*} Sergei Nayakshin² and Q. Daniel Wang³

¹*Instituto de Astrofísica, Facultad de Física, Pontificia Universidad Católica de Chile, 782-0436 Santiago, Chile*

²*Department of Physics and Astronomy, University of Leicester, Leicester LE1 7RH, UK*

³*Department of Astronomy, University of Massachusetts, Amherst, MA 01003, USA*

Accepted 2015 March 14. Received 2015 March 4; in original form 2014 July 10

ABSTRACT

We present numerical models of the gas dynamics in the inner parsec of the Galactic Centre. We follow the gas from its origin as stellar winds of several observed young massive stars, until it is either captured by the central black hole, or leaves the system. Unlike our previous models, we include an outflow from the inner accretion flow. Two different kinds of outflows are modelled: (i) an instantaneous-response feedback mode, in which the outflow rate is directly proportional to the current black hole gas capture rate; and (ii) an outburst mode, which is stronger but lasts for a limited time. The latter situation may be particularly relevant to Sgr A*, since there is evidence that Sgr A* was much brighter in the recent past. We find that both types of outflow perturb the gas dynamics near the Bondi radius and the black hole capture rate significantly. The effects persist longer than the outflow itself. We also compare the effects of spherically symmetric and collimated outflows, and find that the latter are far less efficient in transferring its energy to the surrounding gas near the capture radius. Our results imply that accretion feedback is important for non-radiative accretion flows not only within but also outside the capture radius. Steady-state Bondi accretion rate estimates that do not account for feedback outflows overpredict not only the accretion rate on to the black hole but also the capture rate at the Bondi radius itself. Finally, the steady-state assumption under which non-radiative flows have been routinely studied in the literature may have to be abandoned if accretion feedback is bursty in nature.

Key words: accretion, accretion discs – Galaxy: centre.

1 INTRODUCTION

Over the last 20 or so years, an understanding of gas accretion on to black holes at rates much smaller than their Eddington accretion rates, defined here as $\dot{M}_{\text{Edd}} = L_{\text{Edd}}/(0.1c^2)$, emerged. These flows are very different from their high accretion rate counterparts that are thought to be well-described by the standard accretion disc model (Shakura & Sunyaev 1973). Standard discs are cold, dense, massive and geometrically thin. In contrast, the low accretion rate flows are:

(i) non-radiative – the energy generated by viscous torques locally is not radiated away (Narayan & Yi 1994, 1995). This also implies that the discs are geometrically thick (aspect ratio $H/R \sim 1$).

(ii) two-temperature – the low radiative efficiency of the flows is in part due to low densities and in part due to ions and electrons decoupling from each other thermally, with electrons being much

cooler than ions in the innermost region (Shapiro, Lightman & Eardley 1976; Quataert 1998).

(iii) wind-launching – since the flows are non-radiative, they overheat and spew out a large fraction of their mass and energy budget in outflows emerging from all radii (Blandford & Begelman 1999; Begelman 2012).

These so-called radiatively inefficient accretion flows (RIAFs) have been a success story when applied to observations of low-luminosity active galactic nuclei (LLAGN) and Sgr A*, the supermassive black hole (SMBH) in the centre of our Galaxy (Melia & Falcke 2001; Genzel, Eisenhauer & Gillessen 2010), in particular. The accretion flow region of a SMBH can be defined by its accretion radius, $R_A = 2GM_{\text{bh}}/(c_s^2 + \sigma^2)$, where M_{bh} is the black hole mass, and c_s and σ are the hot gas sound speed and the host galaxy 1D velocity dispersion, respectively. Within $R \lesssim R_A$, the gas dynamics should be controlled by the SMBH gravity and the gas angular momentum. For our Galactic Centre, $R_A \approx 0.04 \text{ pc} \approx 1 \text{ arcsec} \approx 10^5 R_{\text{Sch}}$.

Observations of Sgr A* show that only a small, ~ 0.1 – 1 per cent, fraction of gas *thought* to be accreted at the accretion radius is

* E-mail: jcuadra@astro.puc.cl

finally accreted on to Sgr A*, confirming point (iii) above (Marrone et al. 2007; Wang et al. 2013), which has also been found in state-of-the-art numerical simulations (e.g. Yuan et al. 2015). In this paper we call attention to two important issues: (1) all attempts to understand LLAGN and Sgr A* accretion in particular assumed a steady-state picture of the accretion flow, and this may be too simplistic for connecting the data and theory reliably; and (2) effects of the outflows driven by RIAFs may actually be felt beyond the circularized part of the accretion flow, and even beyond the accretion radius.

In this paper we build 3D numerical models of the dynamics of stellar wind accretion on to Sgr A* in the Galactic Centre, for the first time including the effects of an outflow launched from the SMBH. We find that this RIAF *feedback* effect on to the surrounding gas may reduce gas accretion rates on to SMBH further yet. The complete solution to the surprising dimness of Sgr A* may therefore include not only what goes on *within* the RIAF but also how the RIAF affects the surrounding hot gas reservoir.

1.1 Is the accretion flow on to Sgr A* in steady state?

The observations of Sgr A* give us a number of specific reasons to think that the rate at which gas is deposited into the accretion flow region can vary drastically on relatively short time-scales. First of all, the well-known star formation event in the central parsec of the Galaxy (e.g. Paumard et al. 2006) has probably been triggered by a deposition of a massive, $M \sim 10^{4-5} M_{\odot}$ gas cloud in that region (e.g. Nayakshin & Cuadra 2005). This implies that Sgr A* has come a full circle from being a local equivalent of a (short-lived) quasar (Zubovas, King & Nayakshin 2011; Guo & Mathews 2012; Zubovas & Nayakshin 2012) some ~ 5 Myr ago to a champion underluminous AGN now. Indeed, Mou et al. (2014) have recently shown that a very strong outflow ($\dot{M} \approx 0.02 \dot{M}_{\text{Edd}}$) from Sgr A* could have produced the *Fermi* bubbles.

Aside from this rather extreme variability, there are indications that Sgr A* luminosity varied much more recently. X-ray echoes of the region close to Sgr A* show that it was as bright as $10^{39} \text{ erg s}^{-1}$ only a few hundred years ago (e.g. Ponti et al. 2010). While it is not clear at this moment what triggered this change in X-ray luminosity, it is likely that a significant change in the accretion rate on to Sgr A* is required.

Sgr A* is fed by accretion of stellar winds from the young stellar cluster surrounding it. Many of these young stars are in the Wolf-Rayet phase and have mass-loss rates of the order of $10^{-5} M_{\odot} \text{ yr}^{-1}$. Altogether, they provide more than enough material to explain the current accretion on to Sgr A* (e.g. Quataert 2004). Simulations by Cuadra et al. (2006), Cuadra, Nayakshin & Martins (2008) indicate that the capture rate of stellar winds should experience variations of a factor of a few within a time-scale of a couple of hundred years, which corresponds to the orbital period of the closest wind-emitting stars around Sgr A*. Moreover, a fraction of the stellar wind material may form dense clumps, whose stochastic motion produces spikes in the accretion rate on even shorter time-scales of a few years. It is however unclear how much of that short-time variability will affect the accretion on to Sgr A* itself, as the variations will be smoothed out over the viscous time-scale.

The G2 cloud (Gillessen et al. 2012, 2013; Eckart et al. 2013; Phifer et al. 2013) might correspond to one of the cold clumps predicted by the simulations of Cuadra et al. (2008). Such a cloud, if tidally disrupted by the black hole, would likely increase Sgr A*'s accretion rate (Schartmann et al. 2012). Even though the capture rate at the Bondi radius would increase only slightly (Anninos et al.

2012), this would be accretion of denser material with a coherent angular momentum, so it could change the accretion mode and result in a higher accretion rate at the event horizon. During the next decade, we may witness a significant change on Sgr A* accretion flow that could produce an outflow and will certainly illuminate our understanding of low accretion rate flows.

There are alternative models for G2 that identify this source with a star that loses large amounts of mass, perhaps being partially disrupted by Sgr A* (e.g. Murray-Clay & Loeb 2012; Ballone et al. 2013; Scoville & Burkert 2013). Guillochon et al. (2014) in particular make the case that the G2 cloud formed out of the condensation of debris material from the partial disruption of a star. On average, every decade or so, a clump from the debris would reach the inner region. Moreover, Pfuhl et al. (2015) recently reported the orbit of another gas cloud (G1), which is remarkably similar to that of G2, and that would have preceded it by 13 yr. The mass-loading of the inner accretion flow would then be a relatively frequent feature of Sgr A*, and not a one-off event.

2 THE NUMERICAL MODEL

We use the numerical model for the gas dynamics in the Galactic Centre developed by Cuadra et al. (2005, 2006, 2008), which is based on the well-known GADGET-2 (Springel 2005) code used for cosmological simulations. This is an N -body plus SPH (see e.g. Springel 2010) code in which stellar winds are emitted by the young massive stars that orbit at several arcsec from Sgr A*.

The code follows the gravitational and hydrodynamical interactions of the gas in the potential of Sgr A* and its stellar cluster. Adiabatic processes and a radiative cooling function are included. The effect of viscosity is not included, as our simulations do not reach the actual accretion flow. We have developed two different models for Sgr A*'s outflow, which we implemented on top of the Cuadra et al. (2008) set-up and detail in Section 2.2.

2.1 Stellar winds and accretion

In the simulation we include the 30 stars that have been identified as having important mass-loss rates. The stars follow Keplerian orbits around Sgr A*, which are directly, although not completely, constrained by observations (Paumard et al. 2006). In Cuadra et al. (2008) we tested several stellar orbital configurations that were consistent with the observed stellar 2D positions and 3D velocities, and found that they all yield qualitatively similar results. In this study we concentrate on the effect of the outflow from Sgr A*, thus we use only the ‘1disc’ stellar configuration. In this set-up, roughly half of the stars are given the z coordinate (along the line of sight) defined by Beloborodov et al. (2006), which puts them in a well-defined disc of 10 deg thickness. The rest of the stars are given the z coordinate that minimizes the eccentricity of their orbits, resulting in a more isotropic distribution. As a result, none of the stars gets closer than 1.5 arcsec from Sgr A*. The simulations are started with the stars along their orbits, but 1100 yr in the past. When we present results referring to ‘the present epoch’, that corresponds to having ran the model for 1100 yr until the orbits have reached their current observed positions. That time is long enough for the gas dynamics to have reached a quasi-steady state (Cuadra et al. 2008).

The wind properties of each star, namely, their mass-loss rates and wind velocities, are obtained from their spectra, following Martins et al. (2007) and Cuadra et al. (2008). The mass-loss rates are in the range 5×10^{-6} to $1 \times 10^{-4} M_{\odot} \text{ yr}^{-1}$, and the wind velocities are in the range 600–2500 km s $^{-1}$. Notice that this is a

very different regime to that studied for other LLAGN, where the stellar winds are those of AGB and red giant stars, and therefore much slower (e.g. Shcherbakov et al. 2014). Notice also that these stellar wind velocities are comparable to the stellar orbital velocities around Sgr A*, so both components are relevant and are properly included in the models.

Accretion on to Sgr A* is measured from the simulations as the rate at which matter enters a 0.1-arcsec sink radius. By default, that matter is taken out of the computational domain (but see below). In Cuadra et al. (2008) we found that the captured gas had a circularization radius of $\lesssim 0.05$ arcsec, inside the inner boundary of the calculations.¹ Therefore, our simulations are focused on characterizing how the onset of the accretion flow may be affected by an outflow from the innermost regions, where the bulk of the gravitational energy is released, rather than on providing a comprehensive model of the RIAF itself.

2.2 Outflows from RIAFs

Blandford & Begelman (1999) pointed out physical reasons for the formation of outflows from RIAFs. Sadowski et al (2013) have recently simulated accretion and outflows from non-radiative flows, including the effects of strong magnetic fields, and found that the outflow generally breaks on to a collimated jet and a wide angle wind. The former carries most of the energy while the latter carries most of the mass away from the SMBH.

We lack the resolution to model gas flows on such small scales in this paper, therefore we concentrate mostly on isotropic outflows, which may result from an event that is not directly related to the hot accretion process (e.g. tidal disruption of a star or planet or a cold dense gas cloud, Mościbrodzka et al. 2012; Nayakshin, Sazonov & Sunyaev 2012). In addition, due to variability in Sgr A* feeding, it is not clear how a weak jet component (including its orientation) varies with time. It is quite possible that despite being collimated, the jet shocks easily on the surrounding gas in the vicinity of Sgr A* and hence inflates quasi-spherical hot bubbles. Such an outcome is found in the simulations of jet interaction with the ambient ISM of the host galaxy (Wagner, Bicknell & Umemura 2012; Wagner, Umemura & Bicknell 2013). Still, we present a few tests in which the outflow is collimated, with either variable or fixed orientation.

Outflows in a variety of astrophysical objects are launched at velocities of a few times the escape velocity. For the accretion disc this corresponds to a few times the local Keplerian velocity, $v_K = \sqrt{GM/R} \approx 2 \times 10^8 \text{ cm s}^{-1} (R/0.1 \text{ arcsec})^{-1/2}$. Since the bulk of the mechanical energy is likely generated within our sink radius, the expected outflow velocity ranges from 2000 km s^{-1} to $\sim 0.1c$ for the broad component. The jet component could of course drive a relativistic outflow. Such high outflow velocities would pose a serious numerical challenge to us here, so the maximum outflow velocity we model is 10^4 km s^{-1} . This does not present a serious limitation to our results because it is primarily the energy outflow rate that is important for gas dynamics in the problem at hand, as long as the shocked outflow is non-radiative. On the other hand, the energy deposit could happen entirely outside the present simulation box, which is consistent with the lack of evidence for any significant jet-like feature or its interaction with the surrounding.

In the next subsections, we detail the two different models we use to include an outflow from the vicinity of Sgr A* in the simulations.

2.2.1 Instantaneous feedback

We first implemented an instantaneous feedback mode, in which there is a mild outflow which responds to the accretion rate and is present throughout Sgr A* recent history. This is achieved numerically by expelling, instead of accreting, all particles that reach the sink radius, which in this study is kept fixed at $0.1 \text{ arcsec} \approx 10^4 R_{\text{Sch}}$. Note that black holes in RIAFs do accrete some gas, of course, but the accreted gas fraction is thought to be quite small, e.g. < 0.01 – 0.1 of what enters the RIAF at the Bondi radius (e.g. Blandford & Begelman 1999). This justifies that in this model we simply expel all of the gas.

The particles are expelled with a constant velocity that we treat as a free parameter in the range 10^3 – 10^4 km s^{-1} . The mass-loss rate is not a parameter of this model – it is by definition equal to the instantaneous accretion rate at the sink radius. In most simulations the outflow is isotropic, but we also present two cases in which the outflow is collimated: a ‘fluctuating jet’ case in which each particle is expelled in the direction of its angular momentum vector at the moment of capture, and ‘bipolar’ cases in which particles are expelled in a fixed bipolar cone with half-opening angle of 15° .

2.2.2 Outburst

We implemented a second mode of outflow in which we assume that for a period of time lasting 300 yr and ending 100 yr ago Sgr A* was in a state of higher activity, as hinted by X-ray observations (Ryu et al. 2013). We will follow the ADIOS model (Blandford & Begelman 1999, their example vi), and set a fiducial run with outflow velocity $v = 5 \times 10^8 \text{ cm s}^{-1}$ at a radius of $R \sim 10^4 R_{\text{Sch}}$. The outflow rate is $\dot{M}_{\text{out}} = 10^{-4} M_\odot \text{ yr}^{-1}$. These are the values that we would expect for an $\dot{M}_{\text{in}} \sim 10^{-5} M_\odot \text{ yr}^{-1}$ accretion rate at the innermost stable orbit, following an $\dot{M}_{\text{in}} \propto R^{-3/4}$ power-law dependence, as proposed by Blandford & Begelman (1999). Moreover, these numbers give a mechanical power output of $\sim 10^{39} \text{ erg s}^{-1}$, which coincides with the luminosity inferred for that period. In the same way as we modelled the stellar winds (Cuadra et al. 2006), the outflow has a low temperature of 10^4 K , meaning that its energy budget is dominated by its kinetic energy, which gets thermalized once the outflow shocks against the stellar winds.

Numerically, the outflow is produced by temporarily turning the sink particle that represents the central black hole into a source particle, such as the stars. During this active phase, new gas particles are created around the black hole, at the rate and with the initial velocity quoted above. In most simulations the outflow is isotropic, but we also present a ‘bipolar’ case, with a fixed direction and a half-opening angle of 15° .

3 SIMULATIONS AND RESULTS

3.1 Control run

We start by presenting results from the control run, in which no outflow from the inner region is included and the gas that reached the sink radius was simply accreted by the black hole. This run is basically equivalent with the ‘disc’ model presented by Cuadra et al. (2008).

¹ See also the recent study by Bu & Yuan (2014), which suggests the material might not circularize at all.

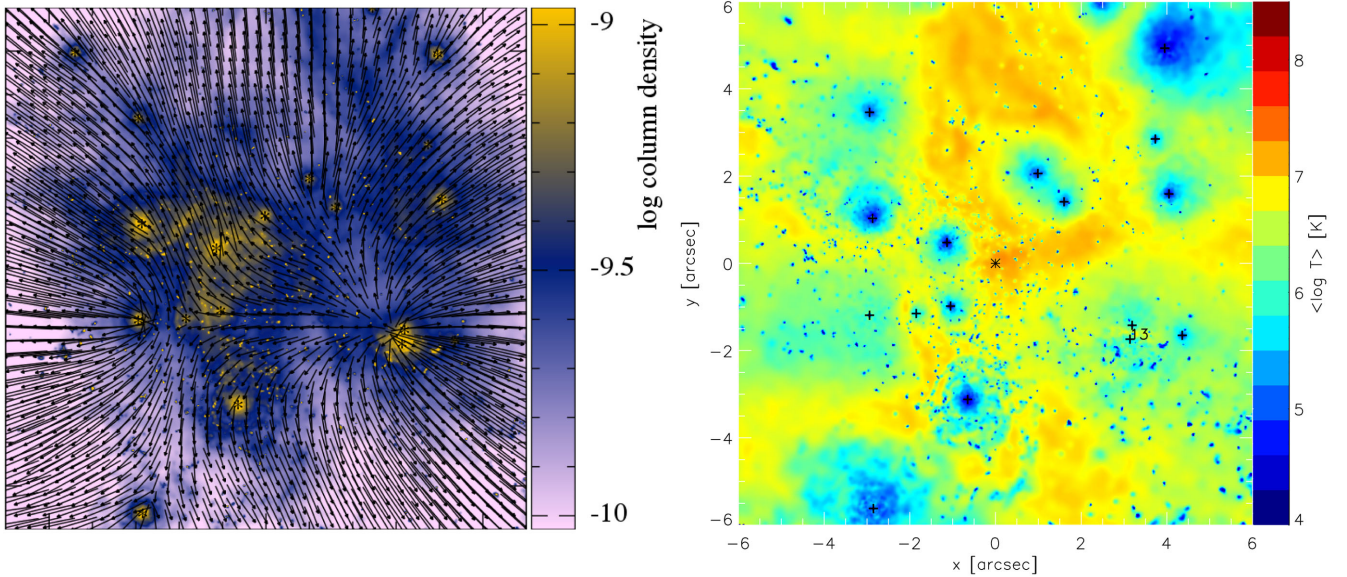


Figure 1. Column density and temperature maps of the control simulation. The maps are 12-arcsec a side and centred on the black hole. On top of the left-hand panel, the projected velocity field is shown with vectors. On the right-hand panel, Sgr A* is shown with an asterisk and stars are shown with small crosses. The IRS13E group is labelled with the number 13.

In the left-hand panel of Fig. 1, we show a surface density map of the control run at the present epoch (i.e. the stars are at their currently observed positions). Notice the overall trend of density decreasing with radius. Besides that, there are local density enhancements around the stars, especially in regions with high stellar densities, where stellar winds collide, and around stars with large mass-loss rates and low outflow velocities, which naturally produce higher gas densities. On top of the density colour map, the arrows show the projected velocity field. Notice that, even in this control run, in most of the map the velocity field can be well-described by a roughly radial outflow, with perturbations due to the effect of some powerful stellar outflows. For this reason, to analyse the effect of the accretion-produced outflow on the velocity field, in this study we will rely on velocity profiles rather than maps.

In the right-hand panel of Fig. 1, we show a temperature map of the same snapshot of the control run. To avoid the hot regions to dominate the averages, each point shows the mass-weighted average of the temperature logarithm along the line of sight, i.e. $\langle \log T \rangle = \int dz \rho \log T / \int dz \rho$, with the integral defined over a range of the same size as the map. In the figure we can see a large range of temperatures, going from the imposed temperature floor of 10^4 K up to $\sim 10^8$ K. The cold gas corresponds to the stellar winds before they collide (when they shock and thermalize), and to dense clumps that form in some of those collisions, due to thermal instabilities (see Cuadra et al. 2008 and Calderón et al. 2015). Most of the shocked stellar winds retain a high temperature and are distributed smoothly over the simulation domain.

3.2 Instantaneous feedback

Here we present the results of the simulations in which we implemented an instantaneous feedback, i.e. there was an outflow proportional to the inflow rate at the sink radius of the simulations, 0.1 arcsec. We use four different values for the outflow velocity, namely $v_8 = v_{\text{out}}/10^8 \text{ cm s}^{-1} = 1, 2, 5, 10$.

We first present in Fig. 2 a density map of the model with the highest outflow velocity, $v_8 = 10$, taken at the current time, so it is

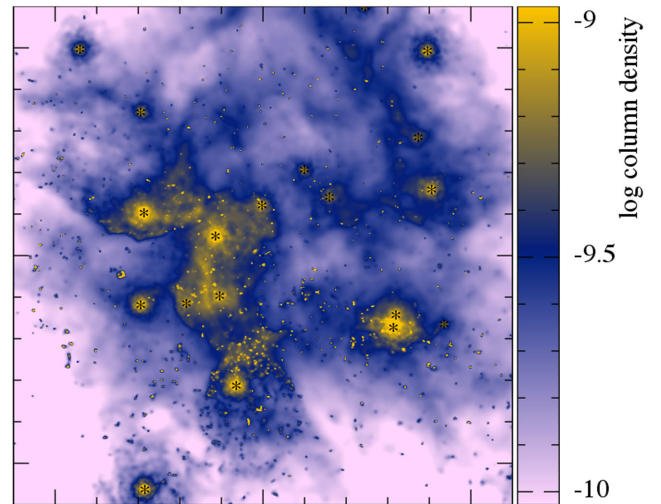


Figure 2. Column density map of the simulation with instantaneous feedback and $v_8 = 10$. The map is 12-arcsec a side and centred on the black hole. Notice the lower density in the black hole vicinity.

directly comparable to the left-hand panel of Fig. 1 from the control run. Notice that the gas morphology is practically the same, except for a small decrement in the inner 1 arcsec region. Within the range of velocities we are exploring, the instantaneous feedback outflow mode does not produce any large-scale signature, like cones or bubbles, and its effect is circumscribed to within the Bondi radius.

Fig. 3 shows the radial profiles of density,² temperature and radial velocity of the gas from the model with $v_8 = 5$. The different lines correspond to snapshots taken at different times in an interval of ± 61 yr from the present time, while the red thick line shows their

² Defined simply throughout the paper as the mass density ρ divided by the hydrogen mass.

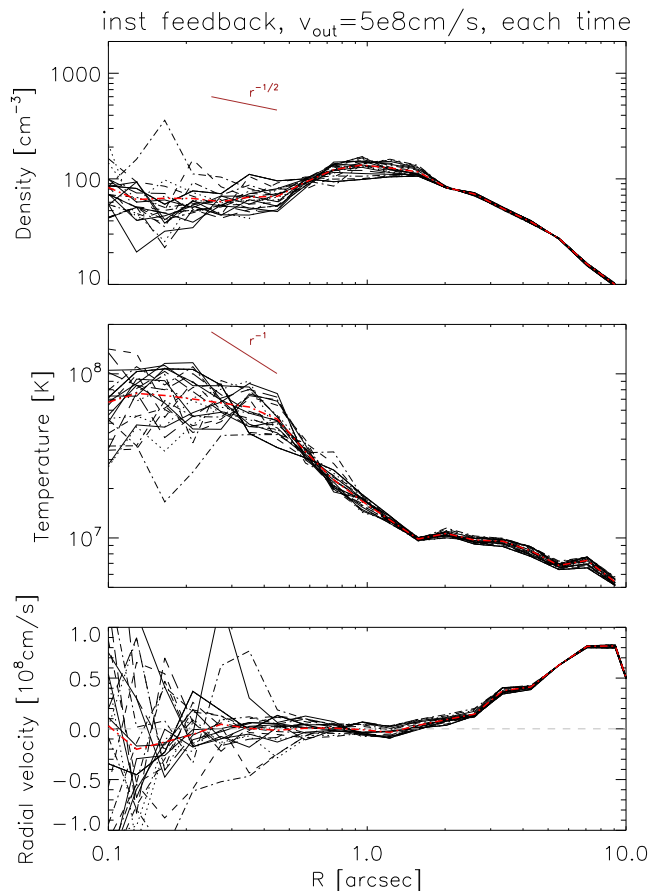


Figure 3. Density (top), temperature (middle) and radial velocity (bottom) profiles of the gas for the run using the instantaneous feedback mode with $v_8 = 5$. Black lines correspond to different snapshots of the simulation, and the red line shows their average. The brown power-law lines in this and the following plots show the observational constraints obtained by Wang et al. (2013), namely, $n \propto r^{-3/2+s}$ with $s \sim 1$, and $T \propto r^{-\theta}$ with $\theta \sim 1$.

average. The average represents well the state of the system for $r \gtrsim 0.5$ arcsec, but the conditions of the gas in the very inner region are highly time-variable and can deviate significantly from the average, in particular the radial velocity. For the rest of the paper, we will use time-averaged profiles in order to compare different simulations, but the reader must be aware that they might deviate somewhat from the state of the system at any given time.

Fig. 4 shows the time-averaged radial profiles for the different simulations. This data visualization allows us to compare among the models better than maps, since the differences are typically only important within the inner 1 arcsec. The profiles are built averaging over 21 snapshots that encompass the present epoch, ± 61 yr. Note that the profiles for the control run differ from simple spherical models (e.g. Quataert 2004) due to the fact that the accreted material originates from a finite number of stars, which are moreover preferentially oriented in a plane (Cuadra et al. 2006). For the cases with $v_8 = 1, 2$ there is an enhancement in the inner density, as the material that would otherwise be accreted is instead launched outwards at the accretion radius. However, since the launching velocity is lower than the escape velocity from the region, the material then stays in that region and therefore there is a density enhancement around the sink radius. In contrast, in the cases $v_8 = 5, 10$, the expelled material is able to escape the inner region and the density does decrease compared to the control run. Overall there's

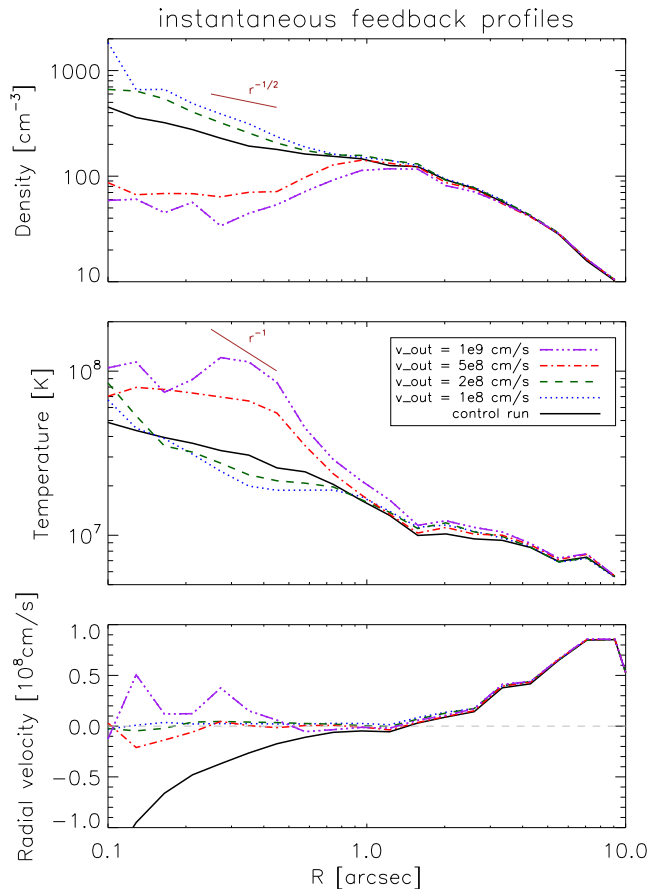


Figure 4. Density (top), temperature (middle) and radial velocity (bottom) profiles for the different runs using the instantaneous feedback mode. The black solid lines show the profiles for the control run, in which no outflow was introduced; the other lines show the profiles for the runs with outflow – see inset legend for details.

a clear trend of higher inner densities for lower outflow velocities. The temperature profiles show higher inner temperatures for higher outflow velocities, due to the additional energy which is injected to the gas which gets quickly thermalized. Notice how the region outside the inner arcsecond is almost completely dominated by the stellar winds – the outflow from Sgr A* only manages to slightly heat up the gas in that region. The two upper panels also show the observational constraints derived from the recent *Chandra* observations of the region around Sgr A*, namely,³ $n \propto r^{-3/2+s}$ with $s \sim 1$, and $T \propto r^{-\theta}$ with $\theta \sim 1$ (Wang et al. 2013). The density profiles favour models with slow or no outflow, while the temperature profiles favour the models with faster outflows. In conclusion, none of these models seem to be consistent with the current data.

The lower panel of Fig. 4 shows the radial velocity profiles. The region where the stars are, $R \gtrsim 1$ arcsec, shows how the stellar winds dominate the dynamics there, and that most of the gas escapes from this region. In the inner part of the flow, we would expect the radial velocity to be null in steady state, as the outflow rate from the inner accretion flow is by construction equal to the inflow rate. However, they do not cancel out exactly due to fluctuations (see Fig. 3). This effect is stronger when the outflow velocity is higher, but notice that the fluctuations are at the level of a few per cent of the outflow

³ Note that the parameters are not determined independently, with $s \sim \theta$.

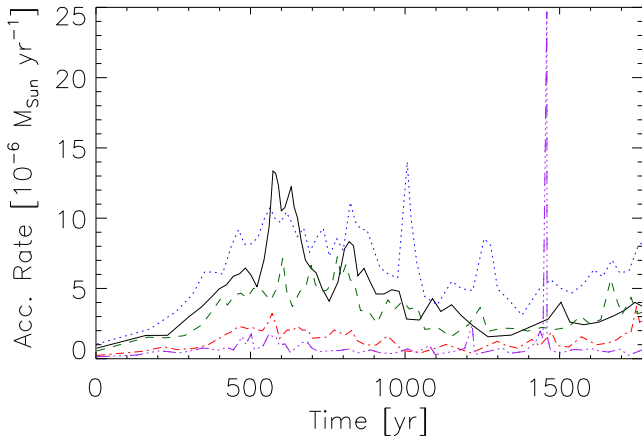


Figure 5. ‘Capture rates’ as a function of time for the different runs using the instantaneous feedback mode. The line meanings are the same as in Fig. 4.

velocity only. This statistical noise also shows up as fluctuations in the density and temperature profiles for the $v_8 = 10$ run. An average over a much larger number of snapshots would be needed in order to smooth these curves out, but that is not needed to draw our conclusions.

Fig. 5 shows the rate at which gas enters the sink radius. For the control run, this corresponds to the accretion rate, as that gas is actually accreted by the sink particle representing the black hole and no outflow is produced at the inner boundary. For the instantaneous feedback runs the gas that reaches that radius is expelled, so the ‘capture rate’ in these simulations describes simply the rate of gas entering the $\sim 10^4 R_{\text{Sch}}$ region rather than Sgr A* accretion directly, which in our model is, by definition, zero. However, it is expected that in reality a fraction of that captured gas be accreted on to the black hole eventually. Therefore, the plotted capture rates do give an idea of the effect of the outflow on regulating the accretion flow boundary conditions.

From the figure, it is clear that higher outflow velocities result in smaller capture rates at the sink radius. The simulation with the lowest velocity, $v_8 = 1$, even shows a higher capture rate than the control run – as that velocity is lower than the escape velocity, the expelled gas remains in the region and can be recaptured by the black hole. In contrast, in the control run the captured gas is accreted by the black hole instead of expelled, and therefore can only be ‘captured’ once. It is worth pointing out that all the runs show nearly identical average physical conditions for the gas at R_A (see Fig. 4), but they differ for up to an order of magnitude in terms of the capture rate at our sink radius, in a 10 times smaller scale. Clearly the Bondi formula cannot be applied when we know that outflows should be produced from within the accretion radius.

Notice also that all capture rate curves are variable, even the one from the control run. This variability is due mostly to the fact that the gas originates from nearby stars, which have non-circular orbits with periods as low as a couple of hundred years. Over such time-scales the stellar configuration changes and that influences the rate of gas that reaches the black hole (Cuadra et al. 2008). Moreover, there is formation of cold ($T \lesssim 10^5$ K) clumps of gas, which sometimes are accreted, as seen at $t \approx 1400$ yr for the $v_8 = 10$ run.

Figs 6 and 7 show the results for runs with $v_8 = 5$ but with different outflow geometries. The isotropic and control runs are the same presented above, the ‘bipolar’ runs correspond to outflows which

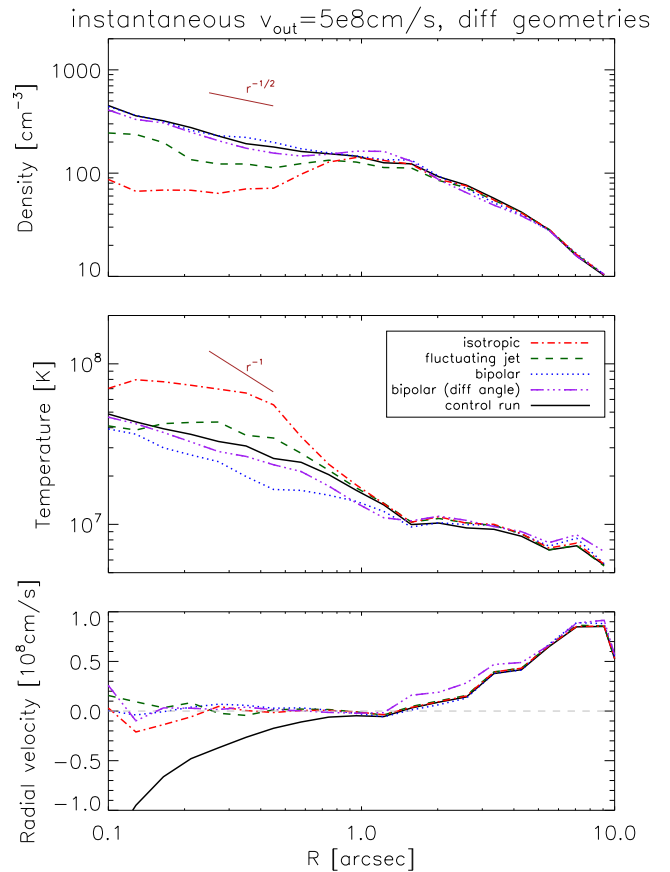


Figure 6. Radial profiles of different gas properties (as in Fig. 4) for the different runs using the instantaneous feedback mode with $v_8 = 5$ and different outflow geometries. The black solid lines shows the profiles for the control run, in which no outflow was introduced; the other lines show the profiles for the runs with outflow – see inset legend for details.

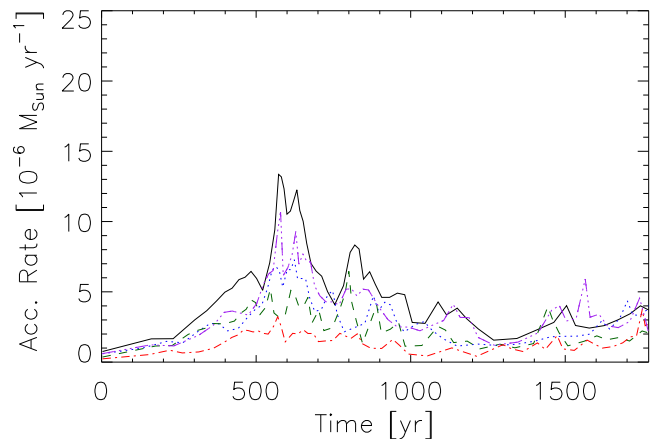


Figure 7. ‘Capture rates’ as a function of time for the different runs using the instantaneous feedback mode with $v_8 = 5$ and different outflow geometries. The line meanings are the same as in Fig. 6.

are confined to a fixed cone with a half-opening angle of 15 deg, and the ‘fluctuating jet’ has each particle ejected in the direction of its angular momentum at the moment of crossing the inner boundary. The results show that the beaming reduces the outflow effect: the density profile and the capture rate for the ‘fluctuating jet’ and

‘bipolar’ cases take intermediate values between the control run and the isotropic run with the same outflow velocity.

3.3 Outburst

In this subsection, we present the results of the simulations in which an outflow lasting 300 yr was added in the model. We concentrate first on a fiducial model with an outflow rate of $10^{-4} M_{\odot} \text{ yr}^{-1}$ and a velocity of 5000 km s^{-1} (see Section 2.2.2). Fig. 8 shows the radial profiles for this run at different times. To avoid fluctuations, each profile is created averaging over 21 snapshots from the simulation, which encompass a period of 122 yr. Thus they are not to be taken as instantaneous states of the system, but as the averages over those periods. We show profiles taken just before the onset of the outflow, during the outflow, and 12–135 and 165–287 yr after the outflow.

Before the outburst we have an unperturbed state in which the density and temperature profiles increase smoothly towards smaller radii. The only substructure present is that produced outside the inner arcsecond by the stellar winds. Note that these profiles differ from the control run profiles of the previous section (see Fig. 4) – here we have a steeper density and a shallower temperature profile. The difference is due to the different times at which the profiles are taken. For the instantaneous feedback profiles we took the system at $t \approx 1100 \text{ yr}$, which, given the stellar positions along their orbits, corresponds to the present epoch. For the outburst simulations, that present time is 100 yr after the outburst finishes, so the ‘before

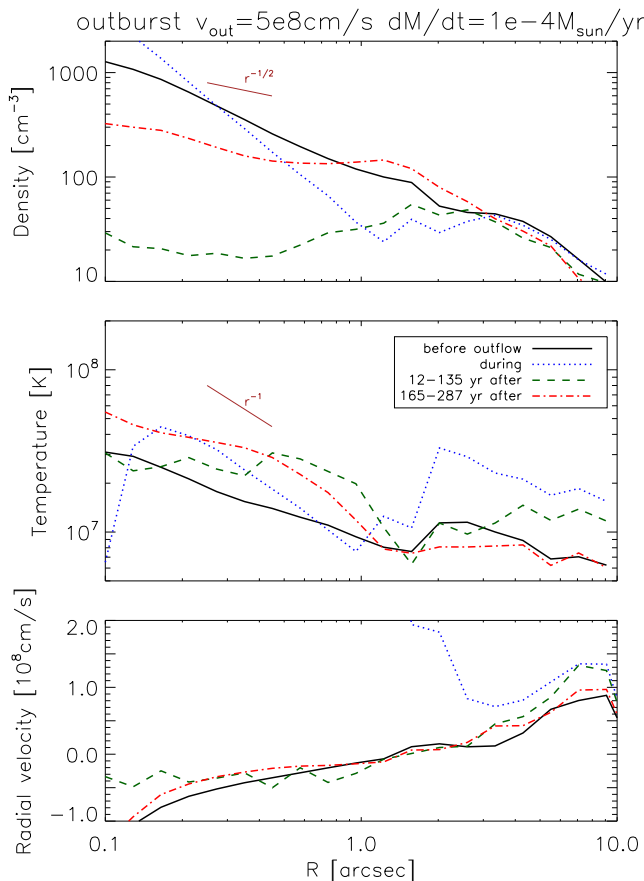


Figure 8. Radial profiles of different gas properties (as in Fig. 4) for the fiducial outburst run at different times – see inset legend for details. While the outflow is active the velocity in the inner region takes the value given as input, out of the plot scale.

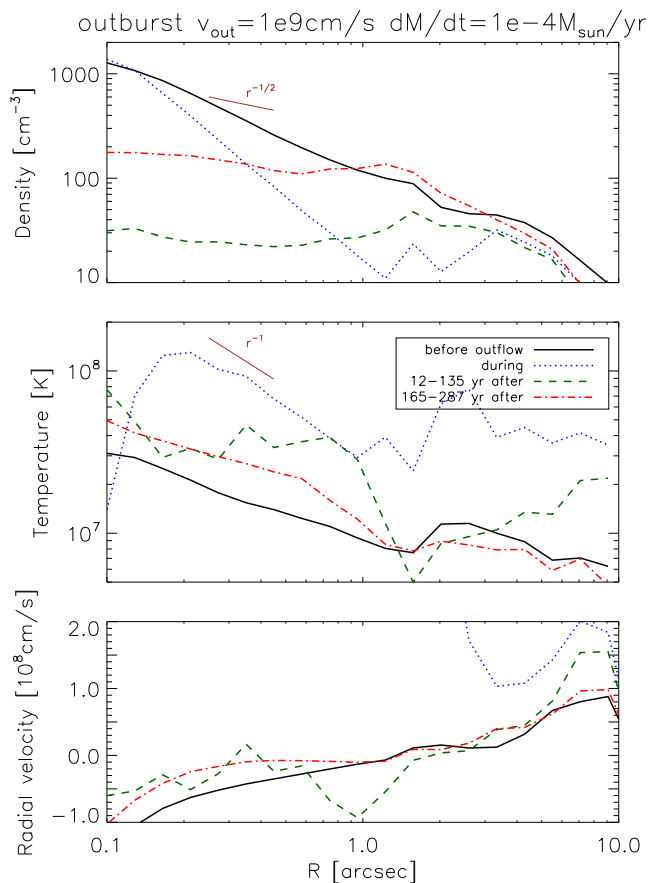


Figure 9. Same as Fig. 8, but for the run with an outflow velocity 10^9 cm s^{-1} .

outflow’ state is at $t \lesssim 700 \text{ yr}$. The different stellar configurations at different times do produce different gas profiles, as it can be inferred from the capture rate versus time plot, Fig. 5.

During the outburst the density profile is very close to an R^{-2} power law, as expected for dynamics completely dominated by an outflow. The temperature shows the formation of a shock front where the outflow from the inner region meets the stellar winds. In the century after the outflow is over, the density in the inner region is strongly reduced compared to its pre-outflow values, but after another 140 yr or so it has mostly recovered. Unlike the instantaneous feedback mode, when the outburst is active, there is no equilibrium between inflow and outflow. That results in a positive radial velocity, as seen in the lower panel of the figure. Either before or after, the inner arcsecond velocity field is dominated by the inflow of the stellar wind material.

In this fiducial run, the density profile gets close to $R^{-1/2}$ during the 165–287-yr time range, at which the temperature profile is almost steep enough to fulfil the observational constraints.

A second simulation had the same characteristics, except that the outflow velocity was twice larger, $10\,000 \text{ km s}^{-1}$. Fig. 9 shows the corresponding profiles. Qualitatively we see a similar behaviour, but there are some interesting differences. During the outflow the density is lower than in the fiducial simulation, which is expected, as \dot{M}_{out} is the same as before and the outflow velocity is higher. Notice also that the influence of the outflow reaches farther out into the region dominated by the stellar winds, with higher temperature and velocity, and lower density, for $R \gtrsim 2 \text{ arcsec}$ while the outflow is active. Moreover, the temperature reached by the gas during

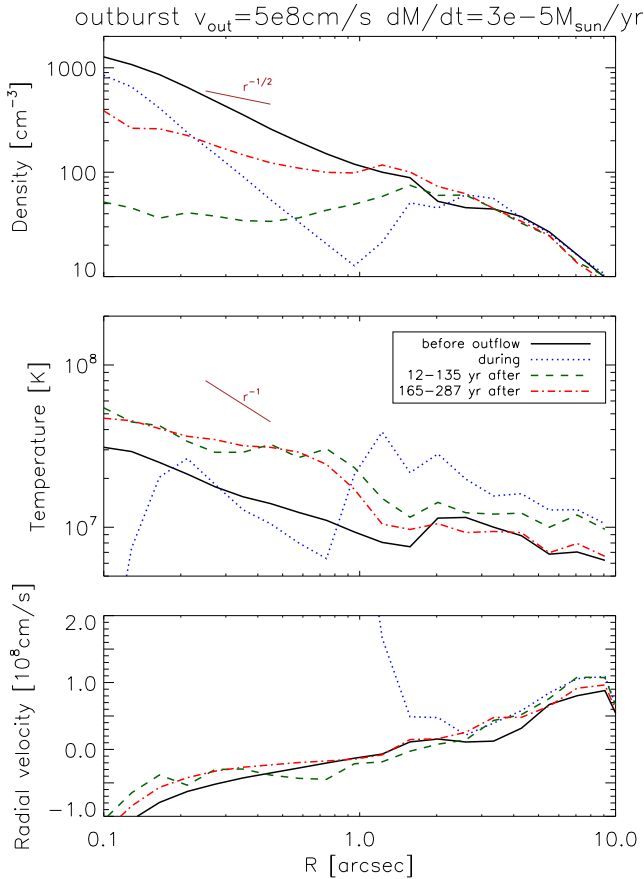


Figure 10. Same as Fig. 8, but for the run with an outburst rate of $3 \times 10^{-5} M_{\odot} \text{ yr}^{-1}$.

and after the outflow are higher, which is consistent with the higher amount of energy injected into the system. The post-outburst density profile is always too shallow to reach the observational constraints.

A third simulation had the same properties of the fiducial run, but three times lower mass-loss rate. The profiles are shown in Fig. 10. As expected, the density is lower during the outflow, and its influence does not reach as far out as in the fiducial run. Moreover, the density profile ‘recovers’ more quickly in this run. However, the temperature profile remains too shallow in most of the radial range of interest, so it cannot meet the observational constraints.

The fourth simulation increased the mass outflow rate by a factor 3 with respect to the fiducial run. As shown in Fig. 11, in this case there is the expected increase in the density and decrease in the temperature during the outflow. After the outflow is over, however, there are no important differences with the fiducial run, except that in this run the density profile remains too shallow to reach the observational constraints over the time-frame of interest.

While all simulations so far had an isotropic outflow, the fifth simulation shown in Fig. 12 shows a variation of the fiducial run but with the outflow confined to a bipolar cone with half-opening angle of 15 deg. Similar as with the instantaneous feedback, this run shows the effect of the outflow to be milder than in the isotropic case. In this run, the density profile at late times is roughly consistent with the observational constraints, but the temperature profile is too shallow. Fig. 13 shows a density map of this model while the outflow is active. Only a small-scale ($R \lesssim 1$ arcsec) conical feature is visible, which quickly disappears once the outflow is turned off.

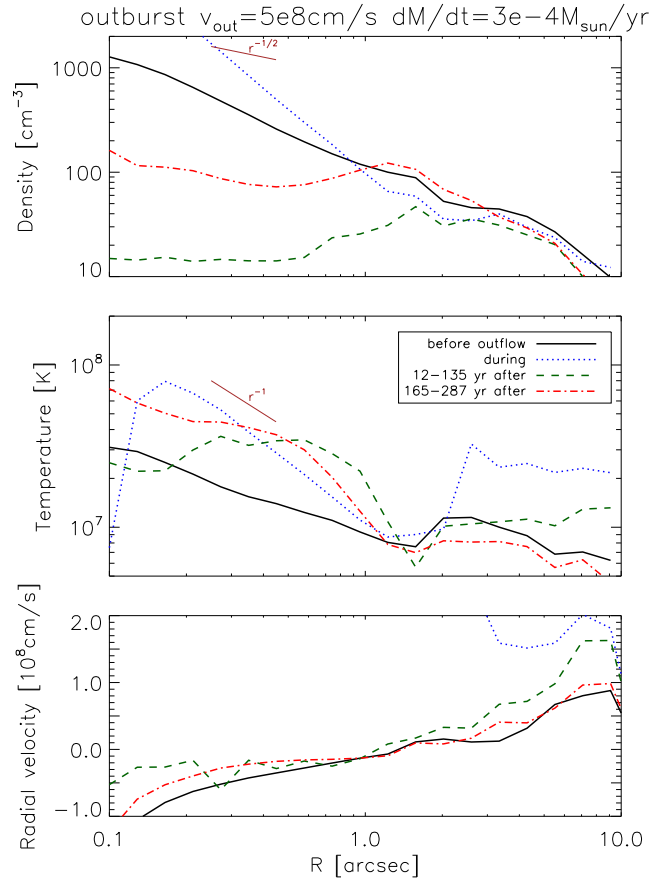


Figure 11. Same as Fig. 8, but for the run with an outburst rate of $3 \times 10^{-4} M_{\odot} \text{ yr}^{-1}$.

Fig. 14 shows the capture rate for the simulations with an outburst presented in this section, together with the control run (without feedback of any kind, same as in Fig. 5). In most outburst simulations, the capture rate goes down to zero while the outburst is active. Then there is a period of 200–300 yr during which the accretion is still suppressed, to come back to values compatible with the control run. That recovery time is roughly the free-fall time of the gas from the location of the nearby stars, ≈ 2 arcsec away from Sgr A*. The only exception to this behaviour is shown by the bipolar run, in which case the capture rate is not completely suppressed and it increases rapidly after the outburst is over.

3.4 Fraction of hot gas

A recent discovery is the high-temperature gas in the so-called Sgr A* halo region (Wang et al. 2013), defined by projected radii in the range 2–6 arcsec. This hot gas could be the result of the outflows we are modelling in this study.

We took the different simulations and calculated the mass fraction of hot ($T > 10^8$ K) gas in that region. The results are plotted in Fig. 15 as a function of time for a few selected simulations. The control run, without any outflows, shows a fraction of hot gas that varies within 0.3–1 per cent. This variation, as that of the accretion rate (Fig. 5), arises from the variations in the stellar configuration due to their orbital motion. The models with an ‘instantaneous feedback’ show a similar pattern, but a slightly higher hot gas fraction – the dotted line in the figure shows the largest effect we achieved in our runs,

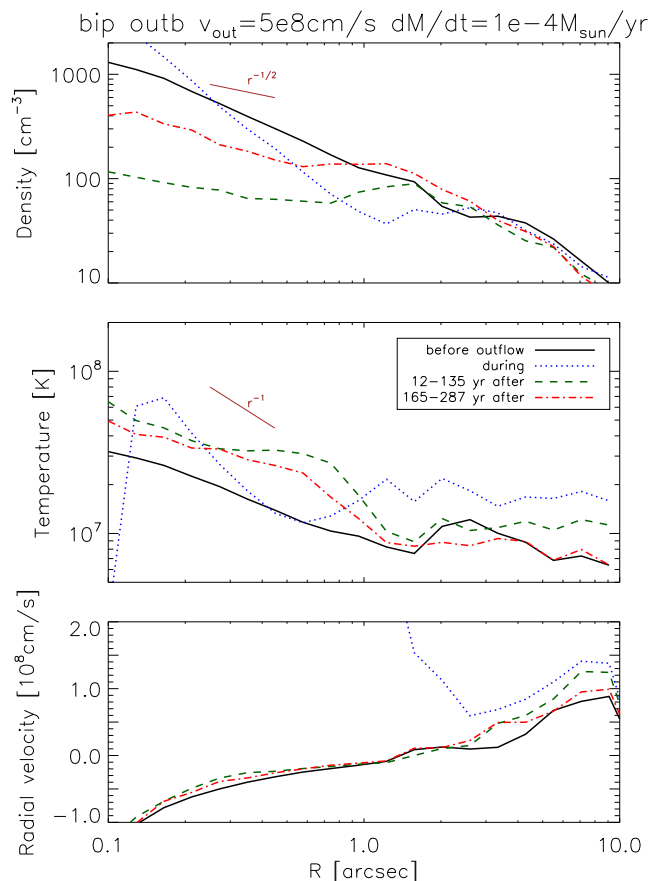


Figure 12. Density (top), temperature (middle) and radial velocity (bottom) profiles for the outburst run with the fiducial values, but a bipolar geometry, at different times – see inset legend for details. While the outflow is active the velocity in the inner region takes the value given as input, out of the plot scale.

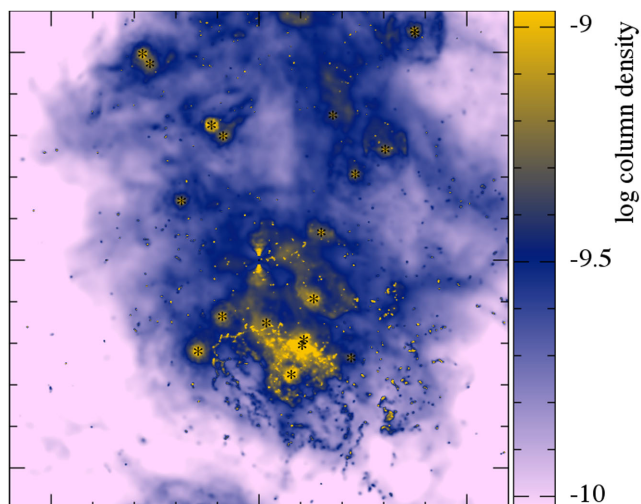


Figure 13. Column density map of the simulation with a bipolar outflow, while the outflow is on. The map is 12-arcsec a side and centred on the black hole. Notice the conical feature at the centre, but the lack of substantial asymmetry further out.

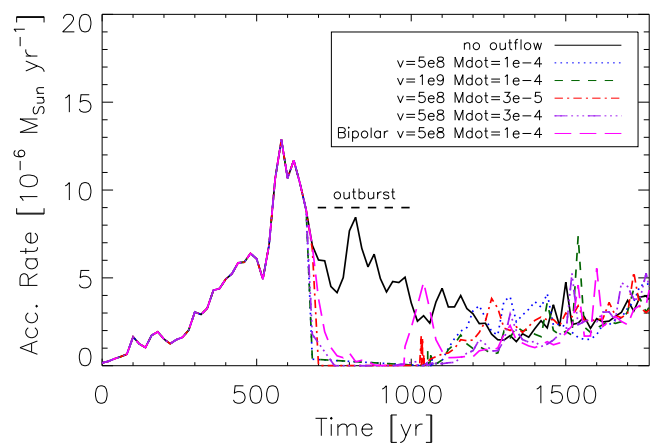


Figure 14. ‘Capture rates’ as a function of time for the different runs using the outburst mode. The solid, black line shows the control run, without outflow. The coloured lines show the results of different runs, using different outflow properties.

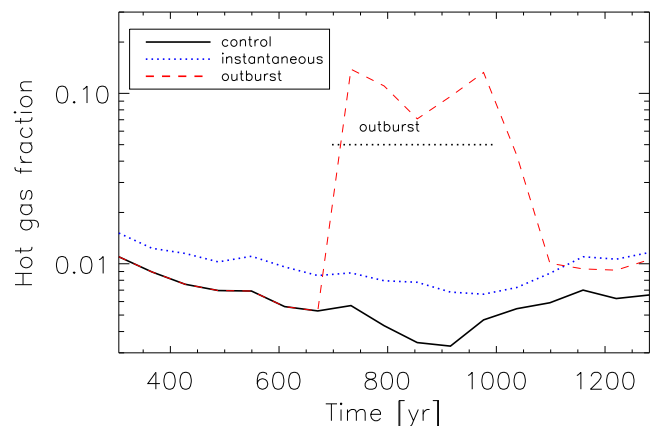


Figure 15. Mass fraction of hot gas as a function of time for different runs. We show the control run, and the simulations that produce the most hot gas for both the ‘instantaneous feedback’ and ‘outburst’ outflow modes.

with $v_8 = 10$. In the simulations that include an ‘outburst’ for the feedback, we see that the fraction increases substantially during the outflow (time interval marked by a horizontal line), reaching values of around 10 per cent for the simulation with outflow velocity $v_8 = 10$ and mass-loss rate $10^{-4} M_\odot \text{yr}^{-1}$. This effect, however, quickly disappears, the mass fraction of hot gas goes back to its pre-outflow value in a hundred-year period after the outflow is over. This is expected, as hot gas has a very large sound speed and quickly leaves this region.

Fig. 16 shows the temperature maps of the simulation with the strongest outflow, both while it is active and at the present time, after the outburst has stopped. It is clear from the left-hand map that the hot gas is distributed throughout the inner computational domain while the outflow is active, and it is only locally hindered by interactions with *stellar* outflows. This gas, as most of the gas outside a 1–2 arcsec radius in all of our models, is outflowing from the computational domain. As discussed above, once the outburst is over, the hot gas quickly leaves the system, and most of the remaining gas is cool, with temperatures comparable to those in the control run (cf. Fig. 1, right).

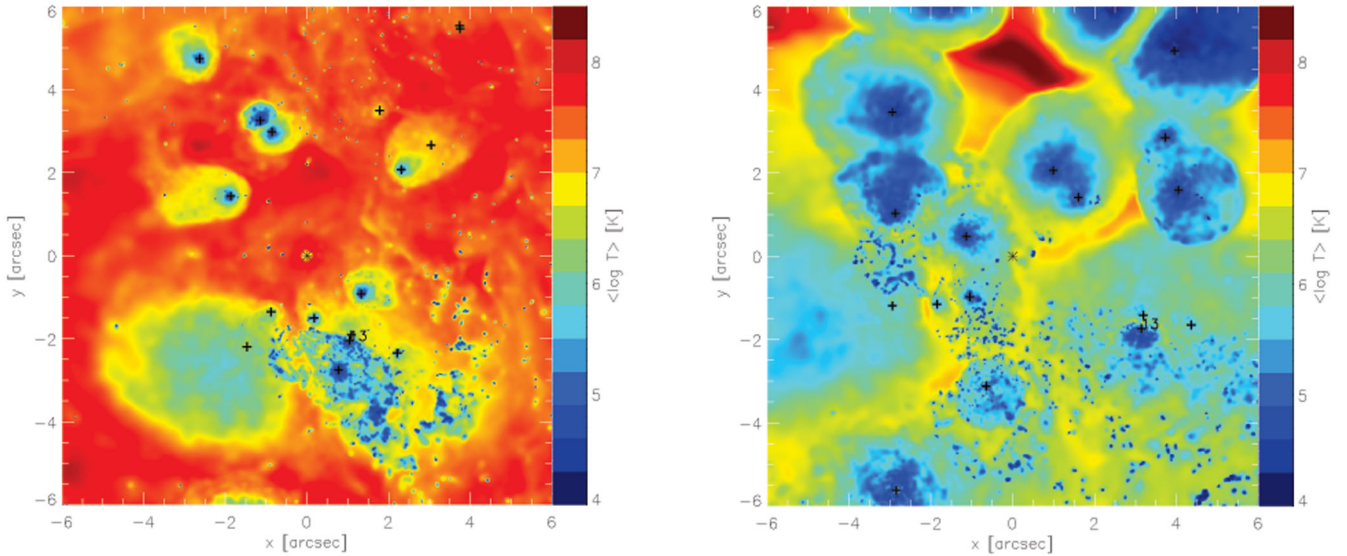


Figure 16. Temperature maps of the simulation with an outburst of $v_8 = 10$ and mass-loss rate $10^{-4} M_{\odot} \text{ yr}^{-1}$. The left-hand panel shows a time when the outflow is active, and a noticeable amount of hot gas is distributed throughout the computational domain. The right-hand panel shows the current time, after the outburst has finished and only a small fraction of hot gas remains. The maps are 12-arcsec a side and centred on the black hole.

4 DISCUSSION

In this study, we have improved our previous models of the Galactic Centre gas dynamics (Cuadra et al. 2008). While those models roughly reproduced the capture rate at the Bondi radius, they were not completely physical in that they ignored the expected presence of an outflow from the inner accretion flow.

We modelled two different types of outflow: (i) an instantaneous feedback, in which material is constantly ejected as it approaches the black hole, and (ii) an outflow which is stronger, but active for a limited time. This latter situation is applicable to sources that went through a recent enhanced black hole accretion episode, which may be the case for Sgr A*. In both cases we found important changes in the dynamics near the capture radius and in the accretion rate. We concentrated mostly on isotropic black hole outflows, but also tested outflows with moderate beaming. In those cases we found the effect of the outflow was reduced, but still noticeable in our models. While the models are specifically tailored for the Galactic Centre, our conclusions are also relevant for other LLAGN, as explained below.

The instantaneous feedback mode shows that the gas at the Bondi radius does not uniquely set the rate at which gas is captured. Models with different outflow velocities (within the relatively narrow range we explored) give accretion rates that differ by a factor of 5, despite nearly identical gas properties at $R \gtrsim 1$ arcsec. On the other hand, the outburst mode shows that our current understanding of Sgr A*'s accretion flow, based on steady-state models, should be revised. If, as believed, Sgr A* was much more active a couple of centuries ago, an outflow of similar power to the inferred luminosity ($\sim 10^{39} \text{ erg s}^{-1}$) could still be affecting the gas we observe at $R \gtrsim 0.1$ arcsec. The accretion rate and gas density at the Bondi radius could still be increasing to pre-outburst values, while the temperature is decreasing. These ‘complications’ add to the ones identified earlier (Cuadra et al. 2008) of variability caused by the orbital motion of the stars around Sgr A* and by the stochastic clump formation.

Overall, the Bondi model, which is symmetrical and time-independent, is not able to account for the complexity of the

accretion-outflow process around Sgr A*. This conclusion is similar to that reached by other authors for LLAGN.⁴ Hillel & Soker (2013) and Shcherbakov et al. (2014) have focused on models for NGC 3115, which is a nearby ($\approx 10 \text{ Mpc}$) LLAGN with an $\sim 10^9 M_{\odot}$ central black hole, meaning that its Bondi radius is easily resolvable (e.g. Wong et al. 2014). Hillel & Soker (2013) argue that the Bondi model is not applicable, as there is central pressure produced by the old stellar population (slow) winds, which originate within the Bondi radius. The 1D numerical steady-state model of Shcherbakov et al. (2014) also includes the effect of stellar winds and supernovae inside the Bondi radius, plus thermal conduction to transport the energy out. Both these models conclude that a time-independent solution is not physical, and that outflows are produced. Note that the physical situation is somewhat different in NGC 3115 compared to our Galactic Centre, as in the latter the stellar wind sources are located roughly at the Bondi radius, and there are no significant stellar sources within (but see Loeb 2004). Nevertheless, the role of the stellar winds in NGC 3115 is comparable to the outflow included in our model.

Due to numerical reasons, our models did not include thermal conduction. The effect of thermal conduction would be to flatten somewhat the density and temperature profiles (Shcherbakov et al. 2014), and it would be mostly circumscribed to the region within the inner arcsecond. It appears that such a flattening would help to reconcile the post-outburst profiles with the observational estimates, so that is in principle an interesting avenue for future research. However, the strong magnetic field likely present in the Galactic Centre (Eatough et al. 2013) would suppress the conduction.

We compared our models with the observational constraints obtained from the recent 3Ms *Chandra* observation of Sgr A* (Wang et al. 2013). None of our instantaneous feedback models fits the

⁴ It is interesting to note that, while the Bondi model overestimates the accretion rate for the case of Sgr A* and LLAGN, in galaxy clusters the Bondi estimate gives too low an accretion rate compared to what is measured for its central AGN (e.g. Cavagnolo et al. 2011), but that is a very different regime to the one we study here.

data, but we find that an isotropic outflow, active ~ 200 yr ago with a rate of $10^{-4} M_{\odot} \text{ yr}^{-1}$ and a velocity of 5000 km s^{-1} , roughly reproduces the currently observed density and temperature profiles. We also rule out any such event happening in the last ~ 100 yr. Our method has therefore the potential to constrain the past activity of Sgr A*, complementing the X-ray echo method which suffers from ambiguity due to the unknown 3D location of the reflecting molecular clouds (e.g. Clavel et al. 2013). These comparisons should be taken at a qualitative level only, as they are based on power-law fits to the observed data and on radial profiles from the simulation data. In a forthcoming paper, we will use the resolved data from both sources to perform a more robust comparison.

Our models show that some gas with very high temperatures remains in the vicinity of Sgr A* for a period of time after the outflow is over. While that cannot explain at face value the recent *Chandra* observations of such hot gas (Wang et al. 2013), it is worth noticing that ours is probably a lower limit. Due to numerical limitations, in our simulations there is an outer boundary condition of free flow at 12 arcsec, while in reality higher density gas on the circumnuclear disc outside that boundary is likely to help in keeping that gas confined. Moreover, we have explored rather mild outflows – for stronger outbursts the amount of hot gas and its temperature would be higher and likely to linger on for longer. Further studies of such outflows and comparisons with observational data will help us constrain the past activity of Sgr A*.

ACKNOWLEDGEMENTS

Density maps were created with *SPLASH*, by Price (2007). We thank the anonymous referee for useful comments that greatly helped us to improve the presentation of the paper. JC acknowledges support from CONICYT-Chile through FONDECYT (1141175), Basal (PFB0609) and Anillo (ACT1101) grants, and the warm hospitality at Leicester. Theoretical astrophysics research in Leicester is supported by an STFC Rolling Grant. QDW acknowledges the support by NASA via the SAO/CXC grant TM3-14006X. This work was performed using the Geryon computers at the Centre for Astro-Engineering UC, funded by Basal PFB-06, QUIMAL 130008 and Fondecuip AIC-57.

REFERENCES

Anninos P., Fragile P. C., Wilson J., Murray S. D., 2012, *ApJ*, 759, 132
 Ballone A. et al., 2013, *ApJ*, 776, 13
 Begelman M. C., 2012, *MNRAS*, 420, 2912
 Beloborodov A. M., Levin Y., Eisenhauer F., Genzel R., Paumard T., Gillessen S., Ott T., 2006, *ApJ*, 648, 405
 Blandford R. D., Begelman M. C., 1999, *MNRAS*, 303, L1
 Bu D.-F., Yuan F., 2014, *MNRAS*, 442, 917
 Cavagnolo K. W., McNamara B. R., Wise M. W., Nulsen P. E. J., Brüggemann M., Gitti M., Rafferty D. A., 2011, *ApJ*, 732, 71
 Calderón C., 2015, MSc thesis, Pontificia Universidad Católica de Chile
 Clavel M., Terrier R., Goldwurm A., Morris M. R., Ponti G., Soldi S., Trap G., 2013, *A&A*, 558, A32
 Cuadra J., Nayakshin S., Springel V., Di Matteo T., 2005, *MNRAS*, 360, L55

Cuadra J., Nayakshin S., Springel V., Di Matteo T., 2006, *MNRAS*, 366, 358
 Cuadra J., Nayakshin S., Martins F., 2008, *MNRAS*, 383, 458
 Eatough R. P. et al., 2013, *Nature*, 501, 391
 Eckart A. et al., 2013, *A&A*, 551, A18
 Genzel R., Eisenhauer F., Gillessen S., 2010, *Rev. Mod. Phys.*, 82, 3121
 Gillessen S. et al., 2012, *Nature*, 481, 51
 Gillessen S. et al., 2013, *ApJ*, 763, 78
 Guillochon J., Loeb A., MacLeod M., Ramirez-Ruiz E., 2014, *ApJ*, 786, L12
 Guo F., Mathews W. G., 2012, *ApJ*, 756, 181
 Hillel S., Soker N., 2013, *MNRAS*, 430, 1970
 Loeb A., 2004, *MNRAS*, 350, 725
 Marrone D. P., Moran J. M., Zhao J.-H., Rao R., 2007, *ApJ*, 654, L57
 Martins F., Genzel R., Hillier D. J., Eisenhauer F., Paumard T., Gillessen S., Ott T., Trippe S., 2007, *A&A*, 468, 233
 Melia F., Falcke H., 2001, *ARA&A*, 39, 309
 Mościbrodzka M., Shiokawa H., Gammie C. F., Dolence J. C., 2012, *ApJ*, 752, L1
 Mou G., Yuan F., Bu D., Sun M., Su M., 2014, *ApJ*, 790, 109
 Murray-Clay R. A., Loeb A., 2012, *Nature Commun.*, 3, 1049
 Narayan R., Yi I., 1994, *ApJ*, 428, L13
 Narayan R., Yi I., 1995, *ApJ*, 452, 710
 Nayakshin S., Cuadra J., 2005, *A&A*, 437, 437
 Nayakshin S., Sazonov S., Sunyaev R., 2012, *MNRAS*, 419, 1238
 Paumard T. et al., 2006, *ApJ*, 643, 1011
 Pfuhr O. et al., 2015, *ApJ*, 798, 111
 Phifer K. et al., 2013, *ApJ*, 773, L13
 Ponti G., Terrier R., Goldwurm A., Belanger G., Trap G., 2010, *ApJ*, 714, 732
 Price D. J., 2007, *PASA*, 24, 159
 Quataert E., 1998, *ApJ*, 500, 978
 Quataert E., 2004, *ApJ*, 613, 322
 Ryu S. G., Nobukawa M., Nakashima S., Tsuru T. G., Koyama K., Uchiyama H., 2013, *PASJ*, 65, 33
 Schartmann M., Burkert A., Alig C., Gillessen S., Genzel R., Eisenhauer F., Fritz T. K., 2012, *ApJ*, 755, 155
 Scoville N., Burkert A., 2013, *ApJ*, 768, 108
 Shakura N. I., Sunyaev R. A., 1973, *A&A*, 24, 337
 Shapiro S. L., Lightman A. P., Eardley D. M., 1976, *ApJ*, 204, 187
 Shcherbakov R. V., Wong K.-W., Irwin J. A., Reynolds C. S., 2014, *ApJ*, 782, 103
 Springel V., 2005, *MNRAS*, 364, 1105
 Springel V., 2010, *ARA&A*, 48, 391
 Wagner A. Y., Bicknell G. V., Umemura M., 2012, *ApJ*, 757, 136
 Wagner A. Y., Umemura M., Bicknell G. V., 2013, *ApJ*, 763, L18
 Wang Q. D. et al., 2013, *Science*, 341, 981
 Wong K.-W., Irwin J. A., Shcherbakov R. V., Yukita M., Million E. T., Bregman J. N., 2014, *ApJ*, 780, 9
 Yuan F., Gan Z., Narayan R., Sadowski A., Bu D., Bai X.-N., 2015, preprint ([arXiv:1501.01197](https://arxiv.org/abs/1501.01197))
 Zubovas K., Nayakshin S., 2012, *MNRAS*, 424, 666
 Zubovas K., King A. R., Nayakshin S., 2011, *MNRAS*, 415, L21

This paper has been typeset from a \LaTeX file prepared by the author.